ELSEVIER

Journal of Nuclear Materials 276 (2000) 221–229

journal of nuclear materials

www.elsevier.nl/locate/jnucmat

Simulation of damage production and accumulation in vanadium

E. Alonso[a,*], M.-J. Caturla[a], T. Díaz de la Rubia[a], J.M. Perlado[b]

[a] *Lawrence Livermore National Laboratory, P.O. Box 808, Livermore, CA 94550, USA*
[b] *Instituto de Fusión Nuclear, José Gutiérrez Abascal, 2, E.T.S.I.I, 28006 Madrid, Spain*

Abstract

Energetic atoms which have been knocked-off their lattice sites by neutron or ion irradiation leave a trail of vacancies and interstitials in their wake. Most of these defects recombine with their opposites within their own collision cascade. Some fraction, however, escape to become freely migrating defects (FMD) in the bulk of the material. The interaction of FMD with the microstructure has long been linked to changes in the macroscopic properties of materials under irradiation. We calculate the fraction of FMD in pure vanadium for a wide range of temperatures and primary knock-on atom (PKA) energies. The collision cascade database is obtained from molecular dynamics (MD) simulations with an embedded atom method (EAM) potential. The actual FMD calculation is carried out by a kinetic Monte Carlo (kMC) code with a set of parameters extracted either from the experimental literature or from MD simulations. Annealing each individual cascade at different temperatures allows the mobile species to escape and account for FMD. We also analyze damage accumulation in a specimen irradiated at low dose rate in the presence of impurities. At the temperature studied, beginning of stage V, we observe that only vacancies are free to move whereas most interstitials are stopped by impurities. We also analyze the role of impurities on damage accumulation and on the concentration of mobile defects.

1. Introduction

Vanadium-based alloys are of great technological importance for future fusion reactors [1]. Their low activation in a 14 MeV neutron environment make them the ideal candidates for the structural material of the reactor first wall. Thus, it is imperative that we fully understand the production and accumulation of radiation damage in these alloys. We present a study of damage production and accumulation in pure vanadium in a first step towards addressing this issue.

Radiation damage production and accumulation in solids can be divided into two stages. In the production stage, the irradiating particle transfers kinetic energy to lattice atoms through elastic collisions. Subsequently, the kinetic energy of the recoils is deposited in the lattice by generating secondary and higher order collisions. At high recoil energies this process results in displacement collision cascades. The outcome of this stage, of the time scale of picosecond, is a population of point and/or clustered defects known as the primary state of damage. In the second stage, which can extend over seconds, defects that survive recombination within their nascent cascade can migrate over long distances, interacting with the microstructure. These freely migrating defects (FMD) are responsible for the changes in the macroscopic properties of metals under irradiation, such as void swelling, embrittlement, radiation enhanced diffusion, etc.

Computer simulation efforts have been conducted in an attempt to model the two stages of radiation damage. Molecular dynamics (MD) simulations studies using many-body potentials of the embedded atom method (EAM) type have proven to be very successful in the description of the first stage of damage production [2,3]. The bulk of the modeling of the second stage has historically been undertaken by rate theory [4–7]. However, the application of kinetic Monte Carlo (kMC) simulations to diffusion processes [8,9] is starting to gain

* Corresponding author. Tel.: +1-925 424 5850; fax: +1-925 422 2118.
E-mail address: ed.alonso@llnl.gov (E. Alonso)

0022-3115/00/$ - see front matter
PII: S0022-3115(99)00181-6

acceptance among the radiation damage community. The main strength of kMC stems from the fact that the highly inhomogeneous nature of the spatial and temporal damage distribution can be easily incorporated and treated. Moreover, features such as one-dimensional migration of small interstitial clusters can also be treated within the same model.

One quantity of fundamental interest for understanding radiation effects in solids is the fraction of FMD. This fraction has been obtained by different experimental methods in the literature. The main approach has been to analyze changes in macroscopic properties believed to depend on the FMD population and to interpret these changes in terms of rate equations. Measurements of radiation-enhanced diffusion [10–14], radiation-induced segregation [15–17], dislocation pinning [18], swelling rates [19], ordering rates [20] and electrical resistivity [21] have been used during the past 20 years to estimate this fraction.

The defects produced during continuous irradiation can annihilate within their own cascade damage (intracascade recombination) or with damage produced by nearby cascades (intercascade recombination) as well as pre-existing defect structures. Therefore, the FMD defined above are only those which escape intracascade recombination. At low dose, the interaction between defects produced in separate cascades is negligible. Thus, the number of free defects is a good approximation to the total number of FMD. At high dose, however, the FMD can interact with the microstructural features generated during irradiation and with those existing prior to irradiation, such as grain boundaries or dislocations. Therefore, the number of FMD which survive intercascade recombination is the parameter which quantifies the number of defects available for interaction with the non-radiation-generated microstructural features.

We present a calculation of the fraction of FMD in vanadium obtained by coupling MD with kMC simulations and compare our results with the experimental data. We also show a simulation of damage accumulation at a fixed dose rate and temperature with varying impurity concentration. The role of impurities will be analyzed in terms of the population of FMD surviving intercascade recombination and damage accumulation behavior.

2. Cascade simulations and defect production

We simulate the primary state of damage by MD simulations. In order to obtain reliable statistics a significant number of cascades has to be produced for each energy. The details of these simulations are shown in Table 1. All MD simulations were performed using the MDCASK code either in its parallel or serial version [22]. All the collision cascades were simulated at room temperature (300 K) and, since little influence on defect production of the irradiation temperature has been observed [2,23,24], the defect configurations were used along the entire temperature range investigated by kMC. The temperature was controlled by connecting the MD box to a thermal bath applying Langevin dynamics [25] to the two outer layers of atoms. The atomic interactions were described by the EAM potential of Johnson and Oh [26]. The short range interaction part was smoothly splined to the universal potential of Biersack and Ziegler [27]. Previous studies with this potential have accurately reproduced the melting point and the displacement threshold energies [28].

Table 1
Computational box size and number of simulations for each recoil energy

Energy (eV)	Box size (lat units)	No. of atoms	No. of cascades
20 000	80×80×80	1 024 000	3
10 000	50×50×50	250 000	6
5000	45×45×45	182 250	4
2000	45×45×45	182 250	7
1000	30×30×30	54 000	9
500	25×25×25	31 250	15
200	25×25×25	31 250	15
100	25×25×25	31 250	15

Due to the open character of the bcc structure, channeling occurred in most of the high energy cascades. Simulations in which channeling caused a cascade to cross the boundaries of the simulation box were eliminated. Only three of the 20 keV cascades were completed out of more than ten started. The simulations were continued until the number of defects reached a stable population. The high melting point of vanadium confines the thermal spike associated with the cascade to a small region that quickly cools. Fig. 1 shows the configuration of the damage produced by a 10 keV recoil after 15 ps. The light points correspond to self-interstitial atoms and the dark ones to vacancies. Vacancies occupy the central part and SIAs the periphery. Only small interstitial and vacancy clusters are formed during this stage and the defects are spread over the simulation box mostly as point defects.

An important result of these simulations is the low interstitial and vacancy clustering observed. We consider a defect cluster to be any group of defects in which each of its members has at least one of the other elements of the cluster in a first nearest neighbor position. Fig. 2 shows the interstitial cluster distribution as a function of recoil energy and cluster size. The largest cluster consisted of seven interstitials in a 2 keV cascade. Except for this cluster, no clusters greater than 3 were observed in cascades below 10 keV. This low clustering is in good

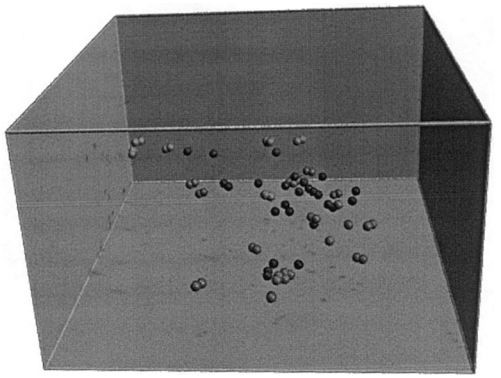

Fig. 1. State of damage generated by a 10 keV PKA at 300 K. The light points represent self-interstitial atoms and the dark ones vacancies. The defect population is stable 15 ps after the PKA entrance. No clusters larger than size 4 are formed.

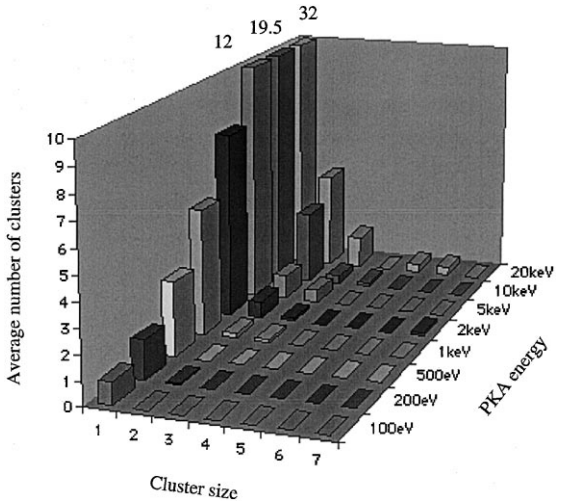

Fig. 2. Average number of interstitial clusters as a function of size and PKA energy. The low clustering tendency is the same for vacancy clusters (not shown in figure).

agreement with previous MD simulations in bcc metals [23,24,28–30].

Another result of these simulations is the effectiveness of the thermal spike in repairing damage, in contrast to the predictions of a purely ballistic model [31]. Fig. 3 depicts the efficiency of the ballistic NRT model to describe damage production. The collisional models break down at high energies because of the local melting of the material [32,33] and the damage production saturates at high energies due to subcascade formation. The efficiency value obtained at high energy recoils is 26%, in good agreement with previous work in bcc [23,24,29,30]. However, the defect production obtained is lower than in the 5 keV cascades at 10 K reported by Morishita and

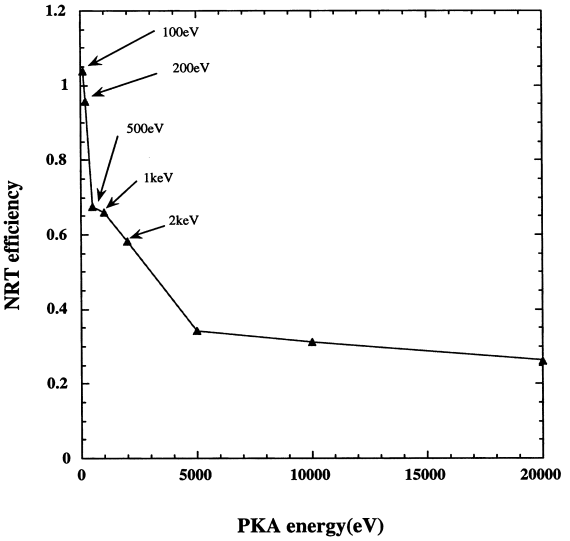

Fig. 3. Efficiency of the NRT model as a function of PKA energy. The small drop from 5 keV (34%) to 20 keV (26%) indicates that the NRT efficiency is close to saturation.

Díaz de la Rubia [28]. The production of self-interstitial atoms (SIA) drops dramatically from 18 at 10 K to 12 at 300 K, which implies a 33% decrease. Still, this is a small difference for such a large range in the temperatures investigated and is therefore in good agreement with the no-temperature-dependence of damage production.

3. Kinetic Monte Carlo simulations

In order to extend the time scale of the simulation we couple the MD output to a kMC code. The kMC simulations were performed with the BigMac code written by Mark Johnson at LLNL [34]. The input needed for the code is the primary state of damage obtained from MD, the diffusivities of the single and clustered defects, and the binding energies of the defect clusters. The input parameters of the model are shown in Tables 2 and 3. All vacancy clusters are assumed to be immobile. The binding energy of vacancy clusters was computed by MD by Shimomura [35]. The formation energy of different cluster configurations was calculated up to size 6

Table 2
Input diffusivities for kMC and reference

	D (cm^2/s)	E_m (eV)	Reference
I	1.0×10^{-3}	0.03	[30]
I2	7.5×10^{-5}	0.067	[30]
I3–I19	1.4×10^{-4}	0.17	[30]
V	1.0×10^{-3}	0.7	[40]

Table 3
Input binding energies for kMC and reference

Cluster size	Vacancy E_b (eV) [35]	Interstitial E_b (eV) [30]
2	0.31	0.71
3	0.58	1.2
4	0.57	2.09
5	1.21	1.67
6	1.19	2.12
7	–	1.84
8	–	3.00
9	–	2.16
10	–	1.96

Vacancy cluster $E_b[n] = 2.17 - 3.15(n^{2/3} - (n-1)^{2/3})$, $n > 6$
Interstititat cluster binding energies (eV)
$E_b[n] = 4.58 - 5.76(n^{2/3} - (n-1)^{2/3})$, $n > 10$
Capture radius for interstitial and vacancy clusters r_c (Å) $= 2.633n^{1/3}$

minimizing the energy by a quasi-newton method [36]. A fit of this curve was made to determine the binding energy as a function of cluster size for larger clusters. The main assumption was that the most stable configuration of large vacancy clusters is purely spherical. Although in pure metals a void will collapse to form a faulted dislocation loop, the presence of helium stabilizes spherical voids. Therefore, the assumption should hold for vanadium, a material with high impurity content and in a helium producing environment. Thus, another point of the curve could be computed for a better fit at large sizes. One perfectly spherical void containing more than 100 atoms was relaxed and its formation energy calculated. As expected under this assumption, the best fit of the formation energy as a function of cluster size is close to a power of (2/3) (Table 3).

The interstitial cluster diffusivities and binding energies are those calculated for iron by Soneda with the EAM potential of Johnson and Oh [26]. Iron and vanadium have a number of important similarities: the same type of lattice and proximity in the periodic table. Moreover, within the context of these calculations both metals are described by the same type of interatomic potential. This factor in particular led us to presume that a detailed study of cluster binding energies and cluster diffusivities in vanadium would yield similar numbers to those of iron. Single-interstitials and interstitial clusters of sizes up to 3 were allowed to migrate three-dimensionally. Interstitial clusters of sizes between 4 and 19 were constrained to one-dimensional migration (glissile) and larger clusters were considered to be sessile.

4. Freely migrating defects

FMD are those defects that escape recombination within their collision cascade. In such a case, the outgoing flux of defects through a spherical surface centered at the cascade and of sufficient radius will account for those defects that are highly unlikely to undergo recombination. Obviously, this definition is sensitive to the radius of the sphere for a given simulation time and temperature. In a real irradiation experiment cascade overlap occurs, so it is reasonable to set the simulation time slightly lower than the time for cascade overlap at a given dose rate. Since the simulation time is fixed by the dose rate and the temperature is a simulation parameter, the only free parameter in our model that can affect the fraction of FMD is the sphere radius. Due to the details of the kMC code, the simulation box is cubic. We compute the fraction of FMD as a function of temperature and recoil energy and analyze the sensitivity of the model to the kMC box size.

The simulation details are as follows. We anneal the primary state of damage obtained in each of the cascades of our database in a kMC box of 100 nm edge for 1000 s. Each of the defects that leave the box are flagged as FMD and removed from the simulation. The simulation size and duration set the maximum cascade production rate to be 10^7 cascades/cm^2 s. In order to improve the statistical validity of the simulation, the calculation was repeated for 100 different random number sequences for each cascade. The same procedure was followed over the temperature range from 150 to 750 K. The fraction of freely migrating interstitials is displayed in Fig. 4 as a function of annealing temperature and PKA energy and the fraction of freely migrating vacancies in Fig. 5. The values shown are

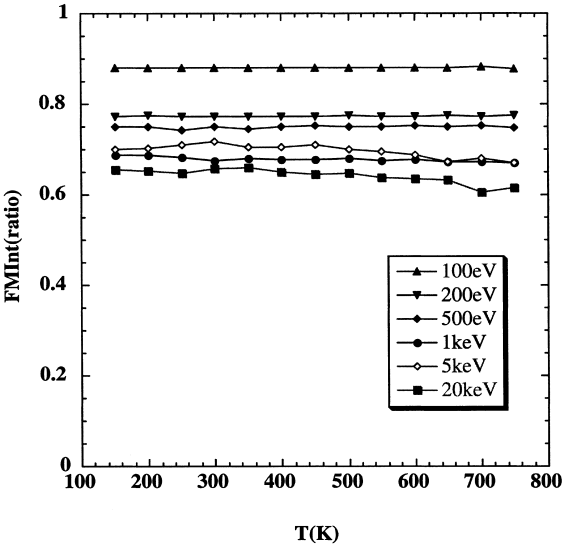

Fig. 4. Escape ratio of interstitials as a function of recoil energy and annealing temperature. Mobile interstitial clusters are also included in the escape ratio. Observe that the escape ratio decreases when the recoil energy increases.

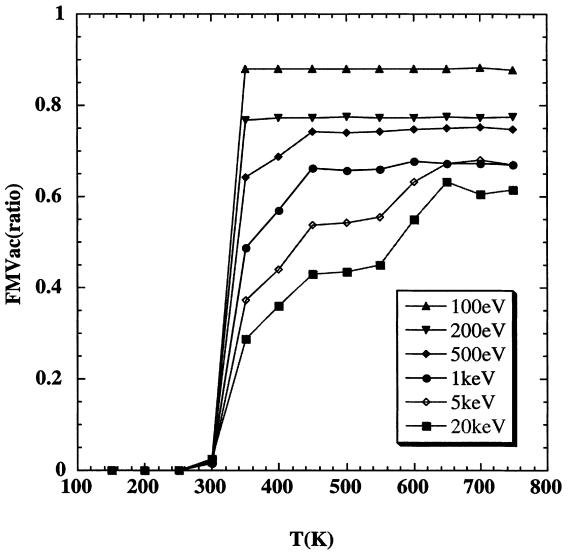

Fig. 5. Escape ratio of vacancies as a function of recoil energy and annealing temperature. The second step corresponding to stage V starts to be visible at PKA energies of more than 1 keV.

averaged over all the cascades available for each recoil energy.

As discussed in Section 4, the largest interstitial cluster observed is of size 7, which is still mobile under our assumption. The high mobility of these clusters results in complete escape from the kMC box over the entire range of temperatures investigated, as seen in Fig. 4. Another interesting feature of this simulation is the correlation between recoil energy and escape ratio. With increasing PKA energy more defects are produced and subsequently more intracascade recombination occurs resulting in a lower escape ratio. This observation is in contrast to similar work on other metals in which the opposite or no dependence was seen [37]. Details of the cascade defect production and clustering fraction as well as the type of lattice may play an important role in this difference. In the referenced study, the material analyzed was gold, a high Z fcc metal. In high Z fcc metals big dislocation loops are formed after the collision cascade and the vacancy rich core is clearly separated from the interstitials in the periphery.

The picture is considerably different for vacancies as shown in Fig. 5. The low diffusivity of the single vacancy means its motion is not noticeable until temperatures of about 270 K, which is 100° above the experimental temperature of stage III in this metal [38]. Stage III temperature is determined by the migration energy of the single vacancy. Unfortunately, the high impurity content of vanadium reflects in wide disagreements over the experimental temperatures of the annealing stages. Moreover, the annealing stages are more tied to impurity migration phenomena than to vacancy migration [39]. These factors led us to use the migration energy calculated by Bacon et al. [40] in the input parameters. Its value of 0.7 eV seems like a good compromise given that experiments report values from 0.5 to 1.2 eV [38]. Therefore, the 100° shift of stage III is a direct consequence of our vacancy migration energy choice. For low energy recoils that is the only feature of the curve due to the absence of immobile vacancy clusters. At high PKA energies only the single vacancies have escaped after stage III has been reached, but small vacancy clusters still remain in the box. Only when the temperature is high enough for those clusters to break-up and emit single vacancies can all the defects escape the box. This happens in stage V, which occurs at the second step located at 550 K in the curves corresponding to the 5, 10 and 20 keV recoils. Once again, this temperature is 100° above the experimental one [39].

The main conclusion of this study is that no production bias of vacancies occurs at any of the temperatures simulated. The fraction of FMD obtained for 20 keV recoils is 17% after normalizing by the NRT model. This number is consistent with previous computer simulations of metals [30,37,41].

The sensitivity of the FMD to the kMC box size was studied. The same simulation was performed for one of the 20 keV cascades, varying the edge of the simulation box from 50 to 200 nm and no appreciable difference in the number of FMD was found. The only difference observed was at the stage III transition temperature. In that temperature regime, the motion of single-vacancies is extremely low and the box size may slightly shift the transition temperature. Some slowly moving vacancies escaped from the small boxes while they did not have enough time in the big ones. This effect is completely negligible.

5. Damage accumulation: intercascade recombination

We perform the following simulation to observe the effect of impurities on damage accumulation and intercascade recombination:

- Dose rate of 10^{-4} dpa/s in a kMC box of 200 nm edge.
- Periodic boundary conditions along the three coordinate axes.
- Flat recoil spectrum of 20 keV.
- Temperature of 650 K, well above the transition temperature for stage V where vacancies clusters become unstable.
- Two spherical sinks with a capture radius of 1.5 nm, both for interstitial and vacancies.
- Presence of interstitial traps.

The traps can be likened to generic impurities. They are immobile, which reproduces a stable population of impurities once steady-state is reached. They are trans-

parent to vacancies but form a tightly bound complex with single-interstitials. Once the impurity–interstitial complex is formed, it can only grow by the arrival of interstitials or shrink by the arrival of vacancies.

We performed the calculation for two different impurity concentrations: 5 and 100 appm. In this way we can single out the role of impurities on the fraction of mobile defects, the cluster density and the clusters size.

Figs. 6 and 7 show the cluster density in both simulations. Damage saturation is quickly reached at about 10^{-3} dpa in the 5 appm case. The cluster density in the 100 appm case keeps increasing linearly at the same dose. These curves are not quantitatively comparable to experiments, not only for the lack of detrapping previously mentioned, but also due to the small size of the clusters in the simulation. As will be explained later, none of the clusters in the simulation should be visible in conventional transmission electron microscopy studies (TEM). Notice also that the concentration of clusters is one order of magnitude greater in the 100 appm case and that the interstitial cluster density approaches asymptotically the impurity concentration in the 5 appm simulation.

The concentration of mobile vacancies during continuous irradiation is plotted as a function of dose in Figs. 8 and 9 for the two impurity concentrations analyzed. Steady-state is quickly reached at both trap concentrations for vacancies and interstitials. As expected, the population of free vacancies is much greater than that of interstitials. According to rate theory, the ratio of the interstitial and vacancy populations is $C_I/C_V \propto D_V k_V^2/D_I k_I^2$ [42]. This is a good approximation for steady-state and sink-dominated absorption of point defects.

The concentration of mobile defects in the 5 appm simulation is five times as much as in the 100 appm one. This is clearly due to reduced recombination with the lower concentration of traps. Traps play an important role on cluster density as well. All the interstitial clusters produced in the collision cascade are of mobile sizes and are rapidly stopped at the traps before they can join and reach sessile sizes. Therefore, the vast majority of interstitial clusters are located at impurity sites. These clusters grow in number and size during irradiation until the saturation of the damage is reached. Saturation takes place when the cluster density approaches its upper limit: the impurity concentration. That is the reason why only 10^{-3} dpa suffice to drive the 5 appm system to damage saturation while the 100 appm one is still in the linear regime. Interstitial cluster growth can be seen in Figs. 10 and 11 for the 5 appm simulation. At the highest dose analyzed (10^{-3} dpa), Fig. 12 shows that the interstitial cluster growth is negligible in the 100 appm simulation.

Vacancy clusters also grow in number but quickly reach a steady average size. After 2×10^{-4} dpa, their size distribution does not change noticeably from the final one in Fig. 11. The average vacancy cluster size oscillates about 10 for the two impurity concentrations. This average value is mainly governed by the simulation temperature. At 650 K, the small vacancy clusters are unstable. Thus, temperature sets the minimum size of stable vacancy clusters. The new-

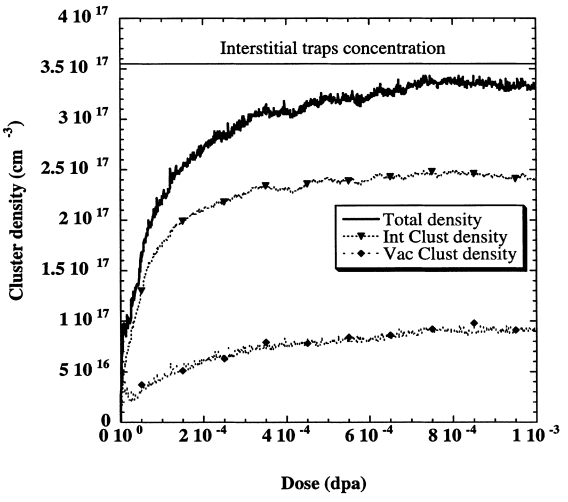

Fig. 6. Interstitial and vacancy cluster density as a function of dose for vanadium with 5 appm impurity content. All the interstitial clusters represented are trapped at the impurities. The number of free interstitial clusters is negligible.

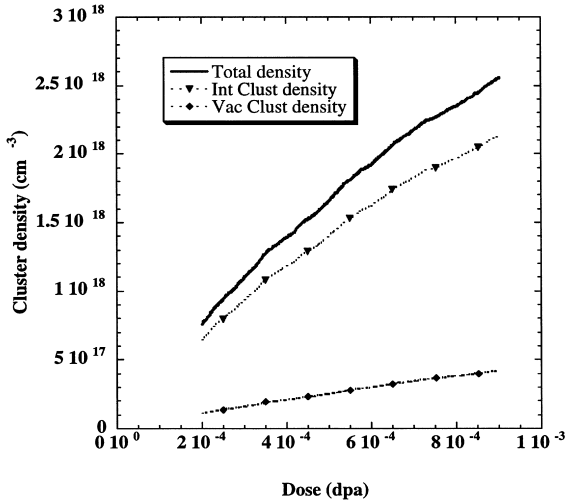

Fig. 7. Interstitial and vacancy cluster density as a function of dose for vanadium with 100 appm impurity content. The damage has not saturated at 10^{-3} dpa because not all the trapping sites have been taken.

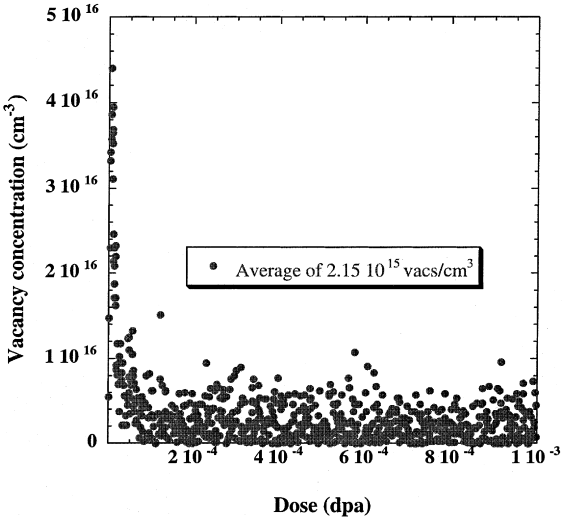

Fig. 8. Mobile vacancies concentration as a function of dose for vanadium with 5 appm impurity content. The average number is 20.

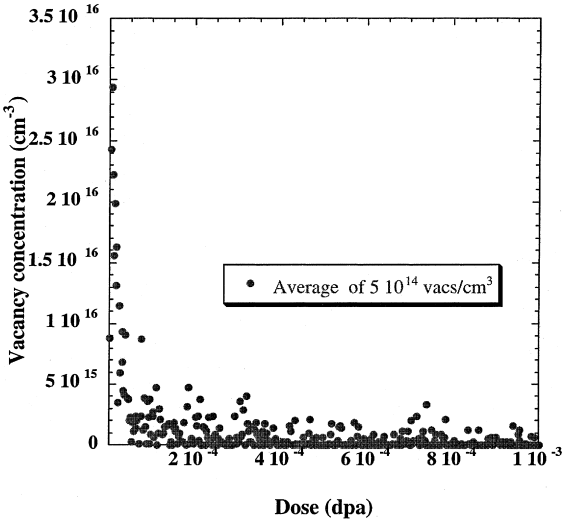

Fig. 9. Mobile vacancies concentration as a function of the dose for vanadium with 100 appm impurity content. The average number is 4 vacancies.

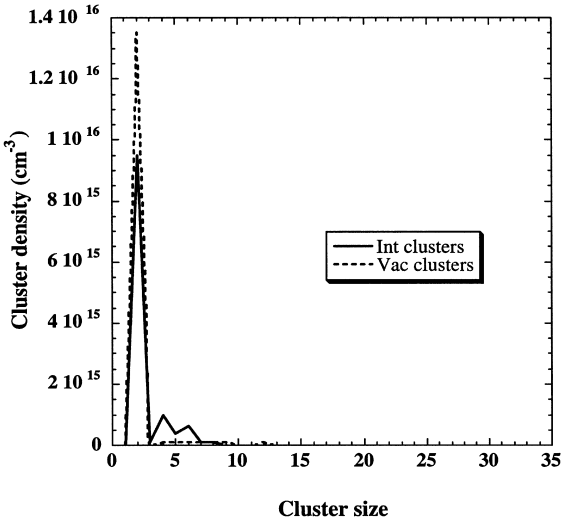

Fig. 10. Cluster size distribution at 10^{-4} dpa in vanadium with 5 appm impurity content.

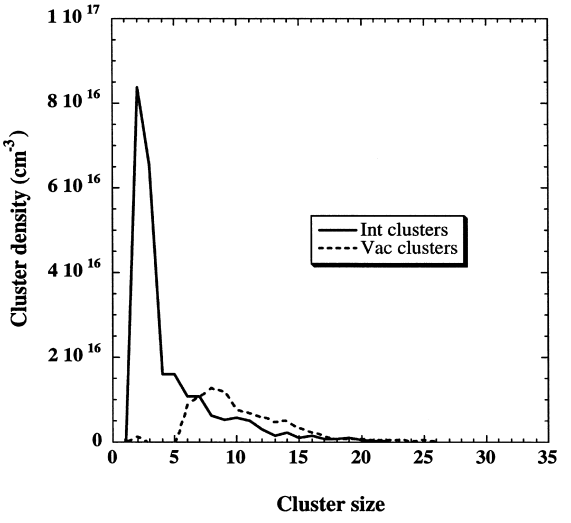

Fig. 11. Cluster size distribution at 10^{-3} dpa in vanadium with 5 appm impurity content. Cluster growth has taken place after the trapping sites have been saturated.

ly produced vacancies are assimilated into new clusters.

The resolution of conventional TEM is ≈1–2 nm; therefore we expect a visible cluster size threshold of ≈40. Since the largest clusters observed have size 27, none of the clusters in our simulation would be visible in the microscope, as pointed out at the beginning of this section.

6. Conclusions

We present an extensive study of damage accumulation coupling MD simulations of damage production and kMC simulations of damage evolution. We calculate the number of defects surviving intracascade (fraction of FMD) and intercascade recombination. We analyze the role of impurities on damage accumulation

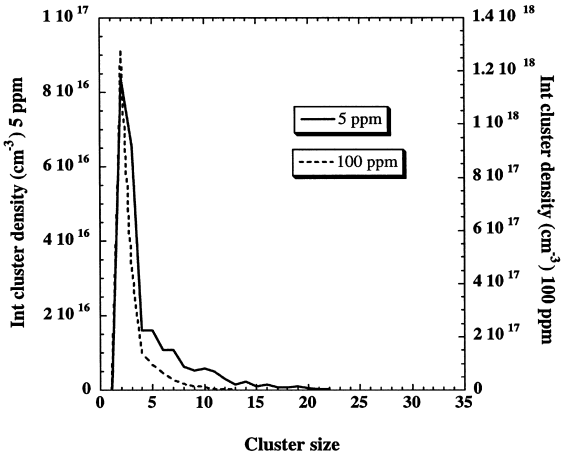

Fig. 12. Interstitial cluster size distribution at 10^{-3} dpa in vanadium with 5 and 100 appm impurity content.

and on the population of mobile defects. The main difference detected is the imbalance in the number of mobile interstitial species and mobile vacancies in the two cases with impurities. This disproportion is the result of the biased nature of the trapping sites and the ratio of the vacancy/interstitial diffusivities. There is a strong correlation between the impurity content and the concentration of mobile species. For vacancies the mobile concentration with 5 appm traps is five times as great as for 100 appm.

In spite of the impossibility of establishing direct comparison with experiments, qualitative conclusions can be drawn on the role of impurities on damage accumulation. The existence of impurities clearly increases the dose required to achieve the saturation of the damage. This saturation is reached in a state in which defect production and recombination are perfectly balanced. Until most of the trapping sites are taken, the trapping contribution is too high to allow equilibrium. Thus, the higher the content of impurities, the longer to reach saturation of damage. Also, the concentration of impurities places an upper limit on the saturation cluster density. The higher the impurity concentration, the higher the cluster density for all doses. Moreover, interstitial clusters coarsen slower with increasing numbers of impurities as shown in Fig. 12. Therefore, the irradiation of materials with high impurity content will result in elevated populations of small obstacles to dislocation motion, with its negative consequences on the embrittlement of the material.

To conclude, interstitial clustering is almost completely governed by traps because of their high mobility. In order to obtain deeper insight into these phenomena and to reproduce experimental conditions in a more realistic manner, work is underway to include the effect of detrapping, real impurities and alloying elements.

Acknowledgements

The authors want to thank Professor Y. Shimomura from Hiroshima University for sharing with them his unpublished data on vacancy cluster binding energies. This work was performed under the auspices of the US Department of Energy by Lawrence Livermore National Laboratory under contract W-7405-Eng-48.

References

[1] H.M. Chung, B.A. Loomis, D.L. Smith, J. Nucl. Mater. 239 (1996) 139.
[2] D.J. Bacon, T. Díaz de la Rubia, J. Nucl. Mater. 216 (1994) 275.
[3] R.S. Averback, J. Nucl. Mater. 216 (1994) 49.
[4] R. Sizmann, J. Nucl. Mater. 69/70 (1968) 386.
[5] R. Bullough, in: Proceedings of the Conference on Dislocations and Properties of Real Materials, The Institute of Metals, Royal Society, London, 1985, p. 382.
[6] H. Trinkaus, B.N. Singh, A.J.E. Foreman, J. Nucl. Mater. 249 (1997) 91.
[7] C.H. Woo, B.N. Singh, A.A. Semenov, J. Nucl. Mater. 239 (1996) 7.
[8] D.G. Doran, Radiat. Eff. 2 (1970) 249.
[9] H.L. Heinisch, J. Nucl. Mater. 117 (1983) 46.
[10] A. Müller, V. Naundorf, M.-P. Macht, J. Appl. Phys. 64 (1988) 3445.
[11] V. Naundorf, M.-P. Macht, H. Wollenberger, J. Nucl. Mater. 186 (1992) 227.
[12] A. Iwase, L.E. Rehn, P.M. Baldo, L. Funk, Appl. Phys. Lett. 67 (1995) 229.
[13] P. Fielitz, M.-P. Macht, V. Naundorf, H. Wollenberger, Appl. Phys. Lett. 69 (1996) 331.
[14] P. Fielitz, M.-P. Macht, V. Naundorf, H. Wollenberger, Z. Metallkd. 87 (1996) 439.
[15] L.E. Rehn, P.R. Okamoto, R.S. Averback, Phys. Rev. B 30 (1984) 3073.
[16] T. Hashimoto, L.E. Rehn, P.R. Okamoto, Phys. Rev. B 38 (1988) 12865.
[17] R.A. Erck, L.E. Rehn, J. Nucl. Mater. 168 (1989) 208.
[18] J.A. Goldstone, D.M. Parkin, H.M. Simpson, J. Appl. Phys. 53 (1982) 4189.
[19] S.J. Zinkle, B.N. Singh, J. Nucl. Mater. 199 (1993) 173.
[20] M.A. Kirk, T.H. Blewitt, Metall. Trans. 9 (1978) 1729.
[21] S.J. Zinkle, J. Nucl. Mater. 155–157 (1988) 1201.
[22] M.W. Finnis, MOLDY 6-A Molecular Dynamics Program for Simulation of Pure Metals, UKAEA Harwell Laboratory, AERE R-13182, 1988.
[23] D.J. Bacon, A.F. Calder, F. Gao, V.G. Kapinos, S.J. Wooding, Nucl. Instrum. and Meth. B 102 (1995) 37.
[24] R.E. Stoller, J. Nucl. Mater. 233–237 (1996) 999.
[25] R. Biswas, D.R. Hamann, Phys. Rev. B 34 (1986) 895.

[26] R.A. Johnson, D.J. Oh, J. Mater. Res. 4 (1989) 1195.
[27] W.D. Wilson, L.G. Haggmark, J.P. Biersack, Phys. Rev. B 15 (1977) 2458.
[28] K. Morishita, T. Díaz de la Rubia, Mater. Res. Soc. Symp. Proc. 396 (1996) 39.
[29] W.J. Phythian, R.E. Stoller, A.J.E. Foreman, A.F. Calder, D.J. Bacon, J. Nucl. Mater. 223 (1995) 245.
[30] N. Soneda, T. Díaz de la Rubia, Philos. Mag. A 78 (N-5) (1998) 995.
[31] M.J. Norgett, M.T. Robinson, I.M. Torrens, Nucl. Eng. Design 33 (1975) 50.
[32] F. Seitz, J.S. Koehler, in: F. Seitz, D. Turnbull (Eds.), Solid State Physics, vol. 2, Academic Press, New York, 1956.
[33] T. Diaz de la Rubia, R.S. Averback, R. Benedek, W.E. King, Phys. Rev. Lett. 59 (1987) 1930.
[34] M.D. Johnson, M.-J. Caturla, T. Díaz de la Rubia, J. Appl. Phys. 84 (1998) 1963.
[35] Y. Shimomura, private communication.
[36] J.B. Gibson, A.N. Goland, M. Milgram, G.H. Vineyard, Phys. Rev. 120 (1960) 1229.
[37] T. Díaz de la Rubia, N. Soneda, M.J. Caturla, E. Alonso, J. Nucl. Mater. 251 (1997) 13.
[38] H. Schultz, Landolt-Börnstein New Series III/25 (1991) 115.
[39] T. Leguey, R. Pareja, E.R. Hodgson, J. Nucl. Mater. 231 (1996) 191.
[40] D.J. Bacon, J.M. Harder, J. Nucl. Mater. 155–157 (1988) 1254.
[41] H.L. Heinisch, Radiat. Eff. Def. Sol. 113 (1990) 53.
[42] C. Abromeit, J. Nucl. Mater. 216 (1994) 78.